3. P. R. Christensen, J. L. Bandfield, M. D. Smith, V. E. Hamilton, *J. Geophys. Res.*, in press.
4. P. R. Christensen *et al.*, *J. Geophys. Res.*, in press.
5. M. D. Smith, J. C. Pearl, B. J. Conrath, P. R. Christensen, *J. Geophys. Res.*, in press.
6. The TES instrument is a Fourier transform Michelson interferometer that covers the wavenumber range from 1700 to 200 cm^{-1} (~6 to 50 μm) at 10 cm^{-1} or 5 cm^{-1} sampling [P. R. Christensen *et al.*, *J. Geophys. Res.* **97**, 7719 (1992)]. The instrument also contains bore-sighted thermal (5 to 100 μm) and visible/near-infrared (VNIR) (0.3 to 3.5 μm) bolometers. The focal planes for the interferometer and the bolometers consist of three cross-track and two along-track detectors with an instantaneous field of view (IFOV) of ~8.5 mrad. The TES instrument uses a pointing mirror that allows for limited targeting capability, limb observations, image motion compensation (IMC), and periodic calibration by observing space and an internal reference surface. The final 2-hour circular mapping orbit of MGS provides a continuous data strip three pixels wide with a spatial sampling of ~3 km by 9 km from a mean altitude of 379 km. The elongated pixel dimension is due to the final mapping orbit of MGS, which crosses the equator at ~2 a.m. local time rather than the intended ~2 p.m. because of damage to the spacecraft solar panel that required lower aerobraking rates. Spacecraft direction relative to the surface is reversed, and IMC does not produce adequate results when stepping the mirror in a direction opposite that originally intended. As a result, spatial sampling is smeared in the along-track direction. These data have improved regional coverage, spatial resolution, and radiometric precision over the aerobraking and science phasing data because of the characteristics of the final MGS 2 p.m. mapping orbit.
7. Christensen *et al.* (*3*) provide a detailed analysis of the uncertainties in atmospherically corrected spectra. For a 280 K surface, the total error in emissivity from random and systematic sources before atmospheric correction is <0.0013 from 300 to 1100 cm^{-1}, increasing to 0.0035 at 1400 cm^{-1} for an average of all six detectors. Random error is lower in the averaged spectra presented here, reducing these uncertainties somewhat. Error due to the atmospheric correction was estimated and is similar to the errors shown in Fig. 1.
8. R. J. P. Lyon and E. A. Burns, *Econ. Geol.* **58**, 274 (1963).
9. G. R. Hunt and J. W. Salisbury, *Environ. Res. Pap. 496-AFCRL-TR-74-0625* (1974).
10. J. W. Salisbury, L. S. Walter, D. D'Aria, *U.S. Geol. Surv. Open-File Report 88–686* (1988).
11. K. C. Feely and P. R. Christensen, *J. Geophys. Res.* **104**, 24195 (1999).
12. M. S. Ramsey and P. R. Christensen, *J. Geophys. Res.* **103**, 577, (1998).
13. M. S. Ramsey, P. R. Christensen, N. Lancaster, D. A. Howard, *Geol. Soc. Am. Bull.* **111**, 646, (1999).
14. V. E. Hamilton and P. R. Christensen, *J. Geophys. Res.*, in press.
15. A. R. Gillespie, *Remote Sensing Environ.* **42**, 137 (1992).
16. J. L. Thomson and J. W. Salisbury, *Remote Sensing Environ.* **43**, 1 (1993).
17. F. D. Palluconi and H. H. Kieffer, *Icarus* **45**, 415, (1981).
18. P. R. Christensen, *J. Geophys. Res.* **87**, 9985 (1982).
19. _____, *J. Geophys. Res.* **103**, 1733 (1998).
20. M. B. Wyatt *et al.*, in preparation.
21. The sample and petrologic analysis were provided by M. B. Wyatt. The glass composition is consistent with rhyolite obsidian with ~75% SiO_2.
22. The least-squares fit algorithm is an iterative program that successively removes concentrations that are less than zero and, therefore, unrealistic. This iterative process may only find a local, rather than global, minimum. Although this raises the possibility of inaccuracies, Feely and Christensen (*11*) and Hamilton and Christensen (*14*) have applied this method extensively and found no adverse or systematic defects due to the iterative process. An additional modification to this algorithm reruns the iterative least-squares fit with only spectral classes found in the final iteration of the algorithm. For example, if the final iteration contains positive concentrations of only diopside and andesine, the algorithm is run again with an end-member set that includes all feldspars and clinopyroxenes that are spectrally similar to andesine and diopside but excludes all other mineral spectra. This commonly improved the fit and reduces the possibility that a correct end-member is accidentally thrown out in the iterative process. The mineral end-member set is currently limited to 400 cm^{-1} and, as a result, the analysis was not performed between 200 and 400 cm^{-1}.
23. Most of the minerals used are from P. R. Christensen *et al.*, *J. Geophys. Res.*, in press. For a complete list, see the supplemental data available at *Science* Online at www.sciencemag.org/feature/data/1047493.shl.
24. V. E. Hamilton, P. R. Christensen, H. Y. McSween Jr., *J. Geophys. Res.* **102**, 25593 (1997).
25. M. S. Ramsey and J. H. Fink, *Bull. Volcanol.* **61**, 32 (1999).
26. The glass end-member used in the analysis is an rhyolite obsidian with a high silica (74% SiO_2) content (*25*).
27. Christensen *et al.* (*3*) performed a similar analysis on a surface spectrum from Terra Cimmeria to test the confidence of minor mineral percentages (<15%).
28. The spectra used were limited to surfaces warmer than 245 K, dust extinctions of <0.25, ice extinctions of <0.15, and RMS fits of measured to modeled spectra of <0.03. Because of the computationally extensive nature of temperature profile retrieval, dust and water-ice opacities were unavailable at the time of analysis. However, although opacity does not correlate perfectly with extinction, low extinctions will limit opacity for surfaces warmer than the atmosphere. Limiting the RMS error of the least-squares fit provides a quick method for filtering highly anomalous data due to errors such as lost bits, mislabeled calibration pairs, and compression errors. These criteria are less restrictive than those used to retrieve the spectral types because the fitting routine is more constrained with fewer end-members. TES emissivity spectra of warm surfaces under a variety of atmospheric and topographic conditions may be modeled with only dust, water-ice, and surface spectral shapes (*1*). While this only provides extinctions, rather than opacities, of atmospheric components, concentrations of each of the surface spectral units may be retrieved (*2*).
29. D. P. Reyes and P. R. Christensen, *Geophys. Res. Lett.* **21**, 887 (1994).
30. H. H. Kieffer *et al.*, *J. Geophys. Res.* **82**, 4249 (1977).
31. M. A. Prestley and P. R. Christensen, *J. Geophys. Res.* **102**, 6551 (1997).
32. C. Sagan, D. Pieri, P. Fox, R. E. Arvidson, E. A. Guinness, *J. Geophys. Res.* **82**, 4430 (1977).
33. H. Y. McSween Jr., *Meteoritics* **29**, 757 (1994).
34. Basaltic Volcanism Study Project, *Basaltic Volcanism on the Terrestrial Planets*, (Pergamon, New York, 1981).
35. J. Gill, *Orogenic Andesites and Plate Tectonics* (Springer-Verlag, New York, 1981).
36. H. Y. McSween Jr. *et al.*, *J. Geophys Res.* **104**, 8679 (1999).
37. P. Toulmin *et al.*, *J. Geophys. Res.* **82**, 4625 (1977).
38. R. Rieder *et al.*, *Science* **278**, 1771 (1997).
39. J. B. Adams and T. B. McCord, *J. Geophys. Res.* **74**, 4851 (1969).
40. R. B. Singer, *Proc. Lunar Planet. Sci. Conf.* **11**, 1048 (1980).
41. R. B. Singer and H. Y. McSween Jr., in *Resources of Near Earth Space*, J. Lewis, M. S. Matthews, M. L. Guerrieri, Eds. (Univ. of Arizona Press, Tuscon, AZ, 1993), pp. 709–736.
42. J. F. Mustard *et al.*, *J. Geophys. Res.* **98**, 3387 (1993).
43. E. Merenyi, R. B. Singer, J. S. Miller, *Icarus* **124**, 280 (1996).

44. We thank H. Moncrief, N. Gorelick, S. Anwar, K. Bender, K. Feely, K. Homan, and G. Mehall for software and operations support and M. Kraft, M. Smith, J. Pearl, W. Stefanov, S. Ruff, M. Wyatt, H. McSween, R. Morris, and J. Holloway for valuable discussions of the results presented here. We also thank the dedicated spacecraft and operations teams at Jet Propulsion Laboratory and Lockheed Martin.

30 November 1999; accepted 19 January 2000

Isotope Fractionation and Atmospheric Oxygen: Implications for Phanerozoic O_2 Evolution

R. A. Berner,[1] S. T. Petsch,[1] J. A. Lake,[2] D. J. Beerling,[2] B. N. Popp,[3] R. S. Lane,[3] E. A. Laws,[3] M. B. Westley,[3] N. Cassar,[3] F. I. Woodward,[2] W. P. Quick[2]

Models describing the evolution of the partial pressure of atmospheric oxygen over Phanerozoic time are constrained by the mass balances required between the inputs and outputs of carbon and sulfur to the oceans. This constraint has limited the applicability of proposed negative feedback mechanisms for maintaining levels of atmospheric O_2 at biologically permissable levels. Here we describe a modeling approach that incorporates O_2-dependent carbon and sulfur isotope fractionation using data obtained from laboratory experiments on carbon-13 discrimination by vascular land plants and marine plankton. The model allows us to calculate a Phanerozoic O_2 history that agrees with independent models and with biological and physical constraints and supports the hypothesis of a high atmospheric O_2 content during the Carboniferous (300 million years ago), a time when insect gigantism was widespread.

A dominant feature of Earth's atmosphere is the presence of abundant free oxygen (O_2), which signifies an active aerobic biosphere. Much attention has been directed toward understanding the rise of O_2 during the Precambrian (*1–5*). Of equal interest, however, is the relative lack of

variability in the partial pressure of atmospheric oxygen (pO_2) during the Phanerozoic (the past 600 million years). Physical and biological constraints based on the fossil record of charcoal and forest fires limit extreme atmospheric composition variations to roughly 10 to 40% O_2 at constant N_2 mass (*6, 7*). This range is remarkably constant considering the potential variation in atmospheric O_2 production and consumption rates that may have occurred over geologic time. On hundred- to thousand-year scales, O_2 is controlled by global rates of photosynthesis and respiration. On longer time scales, the burial of organic matter (OM) and pyrite (FeS_2) in sediments and the oxidative weathering of these materials on the continents (plus oxidation of reduced C- and S-containing gases liberated from them at depth) become the dominant controls on pO_2 (*8, 9*). To maintain approximate constancy of pO_2 through time, strong negative feedbacks must exist within global biogeochemical cycles. Proposed feedbacks include links between pO_2 and forest fires (*7, 10*) and between the concentration of dissolved oxygen $[O_2]_{aq}$ and nutrient availability in the oceans (*11–13*); however, none of these feedbacks have been formulated into a model that is consistent with constraints imposed by chemical and isotopic mass balances for carbon and sulfur.

The calculation of changes in pO_2 on geologic time scales can be achieved if reasonably accurate estimates of burial rates and weathering rates of OM and pyrite can be developed (*14*). Models based on the abundance of organic carbon and pyrite sulfur in sedimentary rocks through time (*15*) provide one approach to the modeling of Phanerozoic pO_2 variations. Another approach is the use of mathematical models driven by carbon and sulfur isotope variations (*9*). In brief, the abundance of ^{13}C in seawater-dissolved inorganic carbon reflects the partitioning of carbon between total global masses of carbonate and OM in sedimentary rocks; likewise, ^{34}S abundance in seawater SO_4^{-} reflects partitioning of sulfur between global sedimentary sulfide and sulfate. These features arise because during photosynthetic fixation of CO_2 there is a strong discrimination in favor of ^{12}C; photosynthetic biomass is significantly depleted in ^{13}C relative to ambient CO_2 (*17, 18*). Analogously, bacterial sulfate reduction exhibits a strong discrimination in favor of ^{32}S; biogenic sulfide minerals are significantly depleted in ^{34}S relative to ambient dissolved sulfate (*19*). Several studies (*16, 20–22*) have attempted to use these features of the carbon and sulfur isotope systems to resolve pO_2 variations based on the isotopic records of marine carbonates and sulfates, which serve as proxies for oceanic values of $^{13}C/^{12}C$ and $^{34}S/^{32}S$. None has generated a Phanerozoic O_2 history that is consistent with physical and biological constraints or the rock abundance model. Indeed, the use of geologically and biologically reasonable feedbacks in isotope-driven O_2 models results in unavoidable positive feedbacks and catastrophic modeled O_2 histories (*16, 23*).

The possible dependence on pO_2 of net carbon isotope discrimination during photosynthesis and biogenic sulfide production are two potentially important factors currently omitted from isotope-driven O_2 modeling studies, although theoretical considerations indicate that both are likely. Increased rates of plant photorespiration under high ambient O_2/CO_2 are predicted because of the dual carboxylase-oxygenase function of Rubisco (*24*), potentially leading to a greater fraction of biomass being derived from ^{13}C-depleted respired CO_2 (*25*). Sulfur cycling in marine sediments is related to O_2 availability, and more recycling results in a greater net biogenic sulfide ^{34}S depletion (*19*). Therefore, to address the sensitivity of these current uncertainties on Phanerozoic O_2 change, we report results from experiments determining the influence of elevated pO_2 on the net ^{13}C discrimination of a herbaceous angiosperm (*Ranunculus repens*), a cycad (*Macrozamia communis*), and a marine diatom (*Phaeodactylum tricornutum*), all grown in the laboratory under a variety of CO_2 and O_2 concentrations. These data have been used, together with a best-guess estimate of sulfur isotope fractionation with O_2 content, to derive a new mass balance model of O_2 for calculating a revised Phanerozoic O_2 history.

Each species of vascular land plant was grown under similar environmental conditions (i.e., light intensity, temperature, humidity, pCO_2, and nutrient supply) but contrasting atmospheric O_2/CO_2 ratios [21 and 35% O_2 with 330 parts per million (ppm) CO_2] in controlled environment chambers described previously (*26, 27*). The upper pO_2 value was taken to represent a previous upper estimate of the past 300 million years (*15*). Table 1 shows the C isotopic composition, expressed as per mil (‰) deviation from the Pee Dee Belemnite standard, of CO_2 in growth chamber air (δ_{gas}) and of the plant samples (δ_{plant}) grown at ambient and elevated O_2 concentrations and the net carbon isotope discrimination Δ_C $[(\delta_{gas} - \delta_{plant})/(1 + \delta_{gas}/1000)]$. These results show, in line with theoretical expectations, that plants grown at elevated pO_2 (35%) exhibit ^{13}C-depleted biomass relative to plants grown under ambient pO_2 (21%). The depletion, expressed as $\Delta(\Delta^{13}C)$ values in Table 1, averaged 1.4‰ for *R. repens* and 3.2‰ for *M. communis*.

The marine diatom *P. tricornutum* was grown under constant light, temperature, and nutrient supply (and thus had a constant growth rate) but variable $[CO_2]_{aq}$ and $[O_2]_{aq}$ in a continuous culture (chemostat) system described previously (*28*). Oxygen saturation of the solution relative to contemporary atmospheric pO_2 ranged from 106 to 155% (equivalent to equilibrium with an atmospheric pO_2 of 22 to 32.5%), whereas $[CO_2]_{aq}$ varied from 3.7 to 20.1 μmol kg^{-1}. Previous work has demonstrated that carbon isotopic fractionation in marine microalgae varies as a function of both $[CO_2]_{aq}$ and algal growth rate (*28, 29*). The isotopic fractionation for *P. tricornutum* grown under similar ranges of growth rate (μ) and $[CO_2]_{aq}$, but in equilibrium with 21% O_2 (*30*), were compared with the results of the present study in order to determine the effect of varying O_2/CO_2 on isotope fractionation corrected for fractionation due to varying CO_2 (Table 2) (*31*).

The results of the experiments can be ap-

[1]Department of Geology and Geophysics, Yale University, New Haven, CT 06520–8109, USA. [2]Department of Animal and Plant Sciences, University of Sheffield, Sheffield, S10 2TN, UK. [3]Department of Oceanography, School of Ocean and Earth Science and Technology (SOEST), University of Hawaii, Honolulu, HI 96822, USA.

Table 1. Fractionation of carbon isotopes during experimental vascular plant growth. All values are expressed as ‰. $\Delta_C = 1000(1 - \alpha_C) = (\delta_{gas} - \delta_{plant})/(1 + \delta_{gas}/1000)$, where α_C is the fractionation factor, numbers after ± indicate 1σ uncertainties, and values in parentheses indicate the number of individual gas or plant samples.

O_2 (%)	$\delta^{13}C_{gas}$	$\delta^{13}C_{plant}$	Δ_C
	R. repens		
21	−3.2 ± 0.7 (10)	−23.0 ± 0.6 (4)	19.9
35	−5.5 ± 0.8 (10)	−26.7 ± 0.3 (4)	21.3
	M. communis		
21	−4.5 ± 0.9 (15)	−22.3 ± 0.2 (6)	17.9
35	−6.0 ± 0.9 (11)	−27.0 ± 1.2 (6)	21.1

Table 2. Carbon isotopic fractionation for the marine diatom *P. tricornutum* grown under different levels of $[O_2]_{aq}$ and $[CO_2]_{aq}$ but at a constant growth rate μ of 0.60 per day. The predicted (Pred.) values for Δ_C were calculated from the data and model of Laws *et al*. (*30*) for *P. tricornutum* for the same values of $\mu/[CO_2]_{aq}$ but for constant present atmospheric pO_2 (21%). Obs., observed. Values of Obs.-Pred. represent changes in fractionation due to varying $[O_2]_{aq}/[CO_2]_{aq}$ corrected for isotopic fractionation due to varying $[CO_2]_{aq}$. For the method of Δ/Δ_C determination, see (*31*).

$[O_2]_{aq}$ (mol kg^{-1})	$[CO_2]_{aq}$ (mol kg^{-1})	$\mu/[CO_2]_{aq}$	$[O_2/CO_2]_{aq}$	Obs. Δ_C (‰)	Pred. Δ_C (‰)	Obs.-Pred. (‰)
260	20.1	0.030	13.0	23.33	23.15	0.18
249	13.1	0.046	19.1	23.28	22.15	1.13
340	3.7	0.162	92.3	22.08	17.35	4.73
362	9.7	0.062	37.5	22.70	21.26	1.44

plied directly to an isotope-driven O_2 mass balance model by calculating the relation between Δ_C and O_2 as

$$\Delta_C \approx \delta^{13}C_{gas} - \delta^{13}C_{plant} = (\Delta_C)_O + J[(O_2/38) - 1] \quad (1)$$

where Δ_C is isotope fractionation (discrimination) for vascular land plant or algal carbon (in ‰); $(\Delta_C)_O$ = 25‰ = Δ_C value for the present level of O_2 but for an average higher-than-present CO_2 level during the Phanerozoic (*32, 33*); O_2 is the mass of oxygen in the atmosphere at any past time; 38 is the mass of oxygen in the present atmosphere (in 10^{18} mol); and J is an empirical coefficient used for curve fitting. Equation 1 closely mirrors that expected from theoretical modeling of photosynthesis and carbon isotope fractionation to the same increase in atmospheric O_2 content (*34*).

Because of the complex effects of oxidation of sulfide and multiple fractionation during diagenetic recycling (*19*), no straightforward experiments on the effects of pO_2 on sulfur isotope discrimination during bacterial sulfate discrimination are possible. As an initial approximation, we assume a simple linear proportionality

$$\Delta_S \approx \delta^{34}S_{sulfate} - \delta^{34}S_{sulfide} = (\Delta_S)_O(O_2/38) \quad (2)$$

where Δ_S is fractionation for sulfur (in ‰) and $(\Delta_S)_O$ is the average fractionation for the present level of O_2 (35‰).

The utility of a model that involves C and S isotopic fractionation depends on how O_2 variations are calculated from carbonate and sulfate isotopic records. Changes with time toward ^{13}C-enriched carbonates indicate an increase in the total mass of OM in sediments and sedimentary rocks, either through increased OM burial or decreased OM weathering. Increased OM burial (or decreased weathering) rates correspond to elevated O_2 production and increasing atmospheric pO_2. However, at constant carbon and sulfur isotope discrimination during biomass production, the variations in atmospheric O_2 calculated from observed variations in the $\delta^{13}C$ of carbonate and $\delta^{34}S$ of sulfate are too large to be realistic, resulting even in highly negative values for pO_2. By allowing photosynthetic carbon and sulfur isotope discrimination to vary with atmospheric O_2, changes in carbonate ^{13}C and/or sulfate ^{34}S content result in damped O_2 variations as compared with O_2 variations derived without the O_2 functionality.

The isotope model used in the present study is that of Garrels and Lerman (*9*), but with O_2-dependent isotope discrimination and the use of both the carbon and sulfur isotopic record to calculate rates of weathering and burial of organic carbon and pyrite sulfur. Also included is rapid recycling analogous to what was done in modeling rock abundance data (*15*). Rapid recycling is a means of incorporating into a model the observation that younger rocks are more likely to be exposed and weathered on the continents than are older rocks. The change in atmospheric oxygen mass (O_2) with time was calculated from the expression

$$dO_2/dt = F_{bg} - F_{wg} + 15/8(F_{bp} - F_{wp}) \quad (3)$$

where F refers to fluxes in mass per unit of time, the subscripts b and w refer to burial and weathering (including oxidation of reduced gases derived from deep processes), and the subscripts g and p refer to organic carbon and pyrite sulfur, respectively.

For carbon isotope fractionation, the values of J in Eq. 1 were varied to obtain an O_2 history bounded between 10 and 40% O_2, which at the same time fitted our experimental plant and plankton growth results (Fig. 1). A curve for J = 2.5 is fit to the experimental data, although a somewhat higher value of J is more likely because cycads [showing the highest $\Delta(\Delta_C)$] represent a primitive life form that is more representative of the burial of ancient terrestrial OM, as emphasized in the present study. Extensive sensitivity analysis showed that the variation of J from 0 to 5 results in a lowering of the peak value of O_2 at 280 million years before the present (My B.P.) (Fig. 2) by about 25% and that values of O_2 for 450 to 350 My B.P. are affected more by the inclusion of O_2 dependence in sulfur isotope fractionation than by its inclusion in carbon isotope fractionation.

The modeling results for the Phanerozoic history of atmospheric O_2 based on Eqs. 1 through 3 and the isotopic composition of sedimentary carbonates (*35, 36*) and sulfates (*16, 37, 38*) as proxies for seawater isotopic composition are shown in Fig. 2 and are compared with the results of the sediment abundance model of Berner and Canfield (*15*). There is surprisingly good agreement between the results of these two totally independent approaches.

The most obvious feature in Fig. 2 is the large pO_2 maximum centered around 300 million years ago, thought to be a response to the evolution of large vascular plants on the continents (*8, 15, 16*). Production of new sources of biomass (such as lignin) that were resistant to the then available pathways of OM degradation likely led to enhanced OM burial in swamps and in marine sediments after transport to the oceans by rivers. This explanation is consistent both with the abundance of coal deposits and OM in general that were preserved at this time (*15, 16*) and with the most severe enrichment in oceanic ^{13}C content measured during the Phanerozoic (*16, 36*).

It has been suggested that variations in globally averaged Δ_C values between sedimentary carbonate and OM correspond largely to variations in atmospheric CO_2 content (*33*). This relation certainly holds for specific classes of organic compounds that show a strong relation

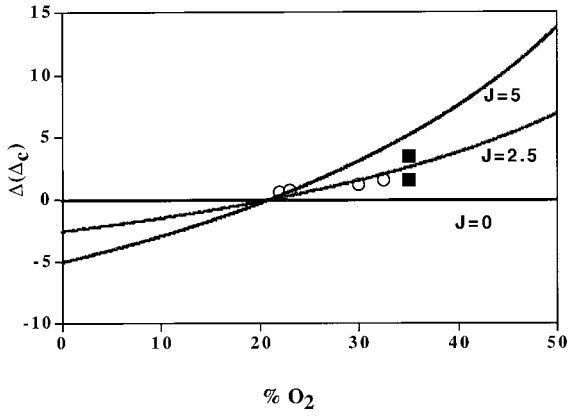

Fig. 1. Plot of carbon isotopic fractionation as a function of % O_2. $\Delta(\Delta_C) = \Delta_C - (\Delta_C)_O$ = change in fractionation from that for 21% O_2. Curves derived from Eq. 1 are shown for different values of J, with the experimental data fitted by J = 2.5. Solid squares represent the vascular plant results of Table 1; open circles are calculated from the data presented in Table 2 for *P. tricornutum* growth in seawater at 25°C equilibrated with 330 ppm CO_2 (*31*).

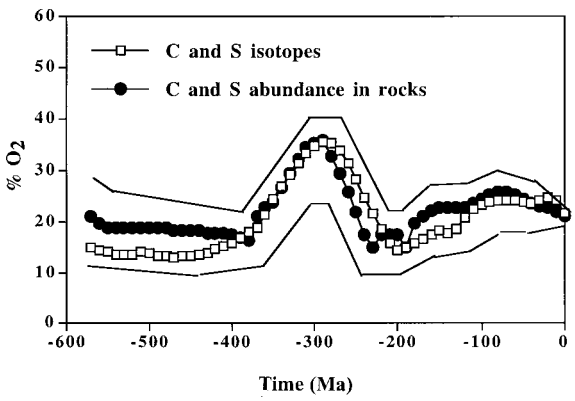

Fig. 2. Plot of O_2 versus time for the Phanerozoic calculated by isotope mass balance modeling (the present study) and by the abundance of organic carbon and pyrite sulfur in sedimentary rocks (*15*). The upper and lower lines represent the range of estimated errors for the results of the rock abundance modeling.

between ^{13}C depletion and ambient pCO_2 values (*39–41*). However, Δ_C values for the Permo-Carboniferous are larger than values immediately before and after this time span, a feature difficult to explain in terms of greatly increased pCO_2. Indeed, Permo-Carboniferous CO_2 concentration is likely to have been decidedly lower than during the preceding and succeeding periods (*32*). The paradox might be resolved if the pO_2 of the Permo-Carboniferous reached 35%, a value indicated by modeling, because a greater measured Δ_C at this time could be explained without relying entirely on the burial of anomalously ^{13}C-depleted OM (*33*). Plant growth experiments demonstrate that plants can grow in atmospheres of up to 40% O_2 (*42*) with the balance between vegetative and reproductive growth remaining unaffected, indicating the possibility of maintaining viable populations under such conditions. Furthermore, a value of 35% O_2 (with $pCO_2 = 300$ ppm) is compatible with continued biogeochemical cycling of carbon by terrestrial ecosystems (*43*). Other physiological studies suggest that elevated pO_2 during the Permo-Carboniferous may help explain patterns in evolution. Flight metabolism in arthropods is enhanced at elevated O_2 concentrations (*44*), and the sudden rise and subsequent fall of insect gigantism documented from the fossil record by, for example, giant dragonflies with wingspans of 70 cm is coincident with the Permo-Carboniferous maximum in pO_2 (*45, 46*). Other patterns have been linked to elevated O_2, such as changes in organisms with diffusion-mediated respiration and the invasion of the land by vertebrates (*45, 46*).

References and Notes

1. L. V. Berkner and L. C. Marshall, *J. Atmos. Sci.* **22**, 225 (1965).
2. P. E. Cloud, *Paleobiology* **2**, 351 (1976).
3. J. C. G. Walker, *Evolution of the Atmosphere* (Macmillan, New York, 1977).
4. H. D. Holland, *The Chemical Evolution of the Atmosphere and Oceans* (Princeton Univ. Press, Princeton, NJ, 1984).
5. D. J. Des Marais, H. Strauss, R. E. Summons, J. M. Hayes, *Nature* **359**, 605 (1992).
6. W. G. Chaloner, *J. Geol. Soc.* **146**, 171 (1989).
7. A. Watson, J. E. Lovelock, L. Margulis, *Biosystems* **10**, 293 (1978); J. M. Robinson, *Palaeogeogr. Palaeoclimatol. Palaeoecol.* **75**, 223 (1989). Watson *et al*. do not allow for O_2 variations to exceed 25%, whereas Robinson states that this value is not well defined and that the maximum O_2 concentration could be considerably higher. For this study, a maximum concentration of 40% was used.
8. H. D. Holland, *The Chemistry of the Atmosphere and Oceans* (Wiley-Interscience, New York, 1978).
9. R. M. Garrels and A. Lerman, *Am. J. Sci.* **284**, 989 (1984).
10. T. M. Lenton, thesis, Univ. of East Anglia, Norwich, UK (1998).
11. H. D. Holland, *Eos* **75**, OS96 (1994).
12. P. Van Cappellen and E. D. Ingall, *Science* **271**, 493 (1997).
13. A. S. Colman, F. T. Mackenzie, H. D. Holland, *Science* **275**, 406 (1998).
14. R. A. Berner and S. T. Petsch, *Science* **282**, 1426 (1998).
15. R. A. Berner and D. E. Canfield, *Am. J. Sci.* **289**, 333 (1989).
16. R. A. Berner, *Am. J. Sci.* **287**, 177 (1987).
17. G. D. Farquhar *et al*., *Aust. J. Plant Physiol.* **9**, 121 (1982).
18. W. M. Sackett, B. J. Eadie, M. L. Bender, A. W. H. Be, *Science* **148**, 235 (1965).
19. D. E. Canfield and A. Teske, *Science* **382**, 127 (1996).
20. L. M. Francois and J. C. Gerard, *Geochim. Cosmochim. Acta* **50**, 2289 (1987).
21. L. R. Kump and R. M. Garrels, *Am. J. Sci.* **286**, 336 (1986).
22. S. T. Petsch and R. A. Berner, *Am. J. Sci.* **298**, 246 (1998).
23. A. C. Lasaga, *Am. J. Sci.* **289**, 411 (1989).
24. D. J. Beerling and F. I. Woodward, in *Stable isotopes. Integration of Biological, Ecological and Geochemical Processes*, H. Griffiths, Ed. (BIOS Publishers, Oxford, 1998), pp. 347–361.
25. J. S. Gillon and H. Griffiths, *Plant Cell Environ.* **20**, 1217 (1997).
26. *R. repens* and *M. communis* seeds were germinated and cultivated on the same medium at 22°C and 70% relative humidity with irradiance of 250 μmol m^{-2} s^{-1}. After 6 weeks (*R. repens*) or 12 weeks (*M. communis*) of growth, seedlings were transferred to controlled growth chambers [design, replication, and environmental regulation detail are given in (*43*)] with either 21 or 35% O_2 and a constant (monitored and controlled) concentration of 330 ppm CO_2. Growth chamber relative humidity was 60 ± 10% and irradiance was 250 μmol m^{-2} s^{-1} under a diurnal cycle of 14 hours of light (at 21°C) and 10 hours of darkness (at 18°C). Plants were watered daily with 40 ml of dilute Rorison's solution.
27. Mature whole leaves were harvested, dried (for 4 days at 30°C), and powdered. (Studies have shown that differences between leaves from different plants or growth conditions are mirrored by the same differences in stems.) Samples were combusted to CO_2 and analyzed in triplicate at the Biomedical Mass Spectrometry Unit, University of Newcastle, UK. Gas samples exiting the growth chambers were collected and CO_2 was isolated and processed as above.
28. E. A. Laws, B. N. Popp, R. R. Bidigare, M. C. Kennicutt, S. A. Macko, *Geochim. Cosmochim. Acta* **59**, 1131 (1995).
29. B. N. Popp *et al*., *Geochim. Cosmochim. Acta* **62**, 69 (1998).
30. E. A. Laws, R. R. Bidigare, B. N. Popp, *Linmol. Oceanogr.* **42**, 1552 (1997).
31. From the relation between $[O_2]_{aq}/[CO_2]_{aq}$ and Obs.-Pred. shown in Table 2, along with the solubility of O_2 and CO_2 in seawater as a function of temperature, we calculated the values of $\Delta(\Delta_C)$ that were appropriate for different pO_2 values and a fixed value of atmospheric CO_2 (330 ppm) and temperature (25°C).
32. R. A. Berner, *Science* **276**, 544 (1997).
33. J. M. Hayes, H. Strauss, A. J. Kaufman, *Chem. Geol.* **161**, 103 (1999).
34. The relation between ^{13}C discrimination and pO_2 is modeled by first calculating the changes in the ratio of intracellular to ambient CO_2 concentration from a coupled photosynthesis model [G. D. Farquhar and S. C. Wong, *Aust. J. Plant Physiol.* **11**, 191 (1984)] and using this ratio to predict ^{13}C discrimination with the well-validated isotope fractionation model given in (*17*).
35. B. N. Popp, T. F. Anderson, P. A. Sandberg, *Geol. Soc. Am. Bull.* **97**, 1262 (1986).
36. J. Veizer *et al*., *Chem. Geol.* **161**, 59 (1999).
37. A. Paytan, M. Kastner, D. Campbell, M. H. Thiemens, *Science* **282**, 1459 (1998).
38. T. B. Lindh, thesis, Univ. of Miami, Miami, FL (1984).
39. B. N. Popp, R. Takigiku, J. M. Hayes, J. Wm. Louda, E. W. Baker, *Am. J. Sci.* **289**, 436 (1989).
40. K. H. Freeman and J. M. Hayes, *Global Biogeochem. Cycles* **6**, 185 (1992).
41. M. Pagani, M. A. Arthur, K. H. Freeman, *Paleoceanography* **14**, 273 (1999).
42. B. Quebedeaux and R. W. F. Hardy, *Plant Physiol.* **55**, 102 (1975).
43. D. J. Beerling *et al*., *Philos. Trans. R. Soc. London Ser. B* **353**, 131 (1998).
44. J. F. Harrison and J. R. B. Leighton, *J. Exp. Biol.* **201**, 1739 (1998).
45. J. B. Graham, R. Dudley, N. M. Aguilar, C. Gans, *Nature* **375**, 117 (1995).
46. R. Dudley, *J. Exp. Biol.* **201**, 1043 (1998).

47. R.A.B. was supported by Department of Energy grant DE-FGO2-95ER14522 and NSF grant EAR-9804781. J.A.L. and D.J.B. gratefully acknowledge funding through a University of Sheffield Alfred Denny research studentship and a Royal Society University Research Fellowship, respectively. Study of carbon isotopic fractionation in marine microalgae at the University of Hawaii has been supported by NSF grants OCE-9301204 and OCE-9633091 to B.N.P., R. R. Bidigare, E.A.L., and S. G. Wakeham and by grant OCE-9521332 to B.N.P. and E.A.L. We thank G. Farquhar, A. Colman, F. Mackenzie, and S. Smith for helpful comments. This is SOEST contribution number 5013.

30 September 1999; accepted 2 February 2000

Natural $NaAlSi_3O_8$-Hollandite in the Shocked Sixiangkou Meteorite

Philippe Gillet,[1]* Ming Chen,[2,3] Leonid Dubrovinsky,[4] Ahmed El Goresy[2]

The hollandite high-pressure polymorph of plagioclase has been identified in shock-induced melt veins of the Sixiangkou L6 chondrite. It is intimately intergrown with feldspathic glass within grains previously thought to be "maskelynite." The crystallographic nature of the mineral was established by laser micro-Raman spectroscopy and x-ray diffraction. The mineral is tetragonal with the unit cell parameters $a = 9.263 \pm 0.003$ angstroms and $c = 2.706 \pm 0.003$ angstroms. Its occurrence with the liquidus pair majorite-pyrope solid solution plus magnesiowüstite sets constraints on the peak pressures that prevailed in the shock-induced melt veins. The absence of a calcium ferrite–structured phase sets an upper bound for the crystallization of the hollandite polymorph near 23 gigapascals.

Alkali feldspars in the system $KAlSi_3O_8$-$NaAlSi_3O_8$ are abundant minerals in Earth's crust. Their behavior under moderate pressure and temperature (*P-T*) conditions is well-known. For instance, the albite to jadeite + quartz transition is a well-calibrated